OPEN

Citation: Cell Death and Disease (2017) 8, e3160; doi:10.1038/cddis.2017.563
Official journal of the Cell Death Differentiation Association

www.nature.com/cddis

A new molecular mechanism underlying the EGCG-mediated autophagic modulation of AFP in HepG2 cells

Lin Zhao[1,6], Shengtang Liu[1,6], Jiaying Xu[1], Wei Li[2], Guangxin Duan[1], Haichao Wang[2], Huilin Yang[3], Zaixing Yang*[,1] and Ruhong Zhou*[,1,4,5]

Epigallocatechingallate (EGCG) is a major bioactive component of green tea and is associated with health benefits against multiple diseases including cancer. As an indicator of hepatocellular carcinoma (HCC), high levels of α-fetal protein (AFP) are related to malignant differentiation and poor prognosis of cancer cells. In this study, EGCG can effectively reduce AFP secretion and simultaneously induce AFP aggregation in human HCC $HepG_2$ cells. EGCG-stimulated autophagy induces the degradation of AFP aggregates in $HepG_2$ cells. Furthermore, we thoroughly studied the underlying molecular mechanisms behind EGCG-stimulated autophagy by using large-scale all-atom molecular dynamics simulations, which revealed a novel molecular mechanism. EGCG directly interacts with LC3-I protein, readily exposing the pivotal Gly-120 site of the latter to other important binding partners such as 1,2-distearoyl-*sn*-glycero-3-phosphoethanolamine and promoting the synthesis of LC3-II, a characteristic autophagosomal marker. Our results suggest that EGCG is critical in regulating AFP secretion and in modulating autophagic activities of $HepG_2$ cells, providing a molecular basis for potentially preventing and treating HCC.

Cell Death and Disease (2017) **8,** e3160; doi:10.1038/cddis.2017.563; published online 2 November 2017

Autophagy is pivotal in various physiological processes. As a highly conserved degradation process of injured protein, lipid, and organelle, autophagy participates in cell growth, development, and death.[1] Autophagy is also a necessary process in bone growth,[2] while suppression of autophagy was related to pathologies, such as cancer.[3] Traditionally, autophagosomal membrane formation is a key process during early autophagic stages. During this process, the microtubule-associated protein 1A/1B-light chain 3 (LC3-I) connects to 1,2-distearoyl-*sn*-glycero-3-phosphoethanolamine (DSPE) through an amide bond with the Gly-120 residue located in the C-terminal region of the former. Then, the formation of lipid-anchored protein LC3-II generates autophagosome production and promotes autophagic activity. When autophagosomes fuse with lysosomes, autolysosomes ultimately form, subjecting damaged organelles and protein aggregates to degradation.[4] Recently, growing interest has focused on exploring the mechanisms of autophagy at the molecular level.

As a healthy beverage consumed worldwide, green tea is historically associated with enormous health benefits against multiple diseases including cancer.[5] Numerous studies have intensively explored epigallocatechingallate (EGCG), which is the most abundant polyphenol in green tea, as a potential therapeutic agent because of its anti-inflammatory, antioxidant, antiobesity, and anticancer activities.[5–7] In addition to advantages of oral administration and limited toxicity, recent studies have used nanoparticles as delivery vehicles to improve the low stability and bioavailability, further promoting the clinical application of EGCG.[8,9] In recent years, the roles of EGCG in mediating apoptotic or autophagy-induced cell death have received great attention, but the findings are controversial. On the one hand, EGCG promotes apoptosis and autophagy in oral cancer SSC-4 cells,[10] and on the other hand, autophagy inhibition contributes to the synergy between EGCG and doxorubicin in a combined treatment of hepatoma Hep3B cells.[11] A recent study also demonstrated that EGCG could attenuate apoptosis and autophagy in concanavalin A-induced hepatitis by inhibiting BNIP3.[12] Therefore, the fact of whether EGCG indeed induces autophagy remains unclear. If EGCG does mediate autophagy, then we need to determine the molecular basis of its mechanism.

α-Fetal protein (AFP) is a major plasma protein produced by the yolk sac and the liver during fetal development, and represents the most abundant plasma protein (40–4000 μg/ml) in the fetus. Although recent studies found that other circulating microRNAs, such as miR-122 and let-7b, performed some similar functions as AFP, AFP still serves as the most common marker in differentiating between hepatocellular carcinoma (HCC) and hepatic cirrhosis.[13] As a prominent biomarker of HCC or germ cell tumors, high AFP level is connected to malignant differentiation, metastasis, and poor prognosis of cancer cells.[14] According to recent statistics, HCC has become one of the leading cancers worldwide, and its mortality is increasing because of the lack of effective treatments against invasion and metastasis.[15] Hence, exploration of potential AFP inhibitors is urgent to protect

[1]School of Radiological and Interdisciplinary Sciences (RAD-X), Collaborative Innovation Center of Radiation Medicine of Jiangsu Higher Education Institutions, Soochow University, Suzhou 215123, China; [2]The Feinstein Institute for Medical Research, 350 Community Drive, Manhasset, NY 11030, USA; [3]Department of Orthopedics, The First Affiliated Hospital of Soochow University, Soochow University, Suzhou 215006, China; [4]Computational Biological Center, IBM Thomas J Watson Research Center, Yorktown Heights, NY 10598, USA and [5]Department of Chemistry, Columbia University, New York, NY 10027, USA

*Corresponding author: Z Yang or R Zhou, School of Radiation Medicine and Protection, Soochow University, 199 Renai Road, Suzhou Industrial Park, Suzhou 215123, Jiangsu, China. E-mail: zxyang@suda.edu.cn or ruhongz@us.ibm.com

[6]These authors contributed equally to this work.

Received 05.5.17; revised 20.9.17; accepted 22.9.17; Edited by B Zhivotovsky

HCC patients from deterioration. Recently, Fang *et al*.[16] showed that silencing of AFP expression by small interfering RNAs resulted in the effective inhibition of hepatoma cell growth and promotion of apoptosis. Houessinon *et al*.[17] reported that sorafenib, a regular HCC chemotherapy drug, could control HCC, and its curative effect was best associated with lower AFP levels. In addition, a novel method combined anti-AFP-coated magnetic Fe_3O_4 nanoparticles with low-frequency electromagnetic field exposure induced the apoptosis of Bel-7402 and $HepG_2$ hepatoma cells lines without manifesting any significant side effects on HL-7702, a normal hepatic cell line.[18] Notably, EGCG could inhibit AFP secretion in human hepatoma-derived PLC/PRF/5 cells[19] and reduces the serum AFP level in HCC rat models.[20] However, the mechanism underlying the way by which EGCG regulates AFP levels in HCC cells remains elusive. By using a combined approach with both experimental and computational techniques, we aim to demonstrate the effect of EGCG on AFP secretion, and more importantly, to reveal the underlying relationship between AFP secretion and EGCG-induced autophagic activities in human HCC $HepG_2$ cells.

Results

EGCG inhibits the growth of HepG2 cells. We used the 3-[4,5-dimethyl-2-thiazolyl]-2,5-diphenyl-2*H*-tetrazolium bromide (MTT) method in our study to analyze the cytotoxic effect of EGCG on $HepG_2$ cells. EGCG inhibited the growth of $HepG_2$ cells in a time- and dose-dependent manner with IC_{50} values between 60 and 80 μM (Figure 1a). At 150 μM, the maximum inhibition of cell growth by EGCG was 50.44%, 69.96%, and 80.38% after 24, 48, and 72 h, respectively.

EGCG reduced AFP secretion in $HepG_2$ cells. We measured intracellular and extracellular AFP content by western blot analysis in $HepG_2$ cells to further determine

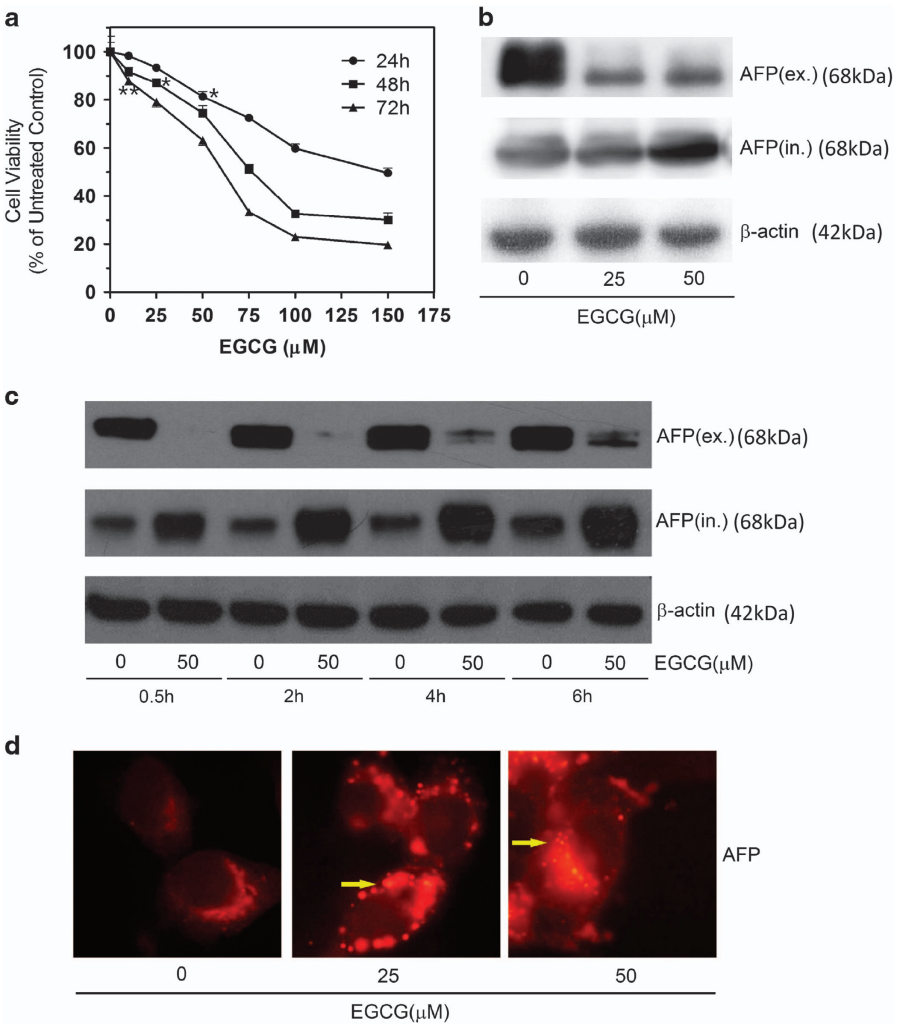

Figure 1 EGCG induces AFP aggregation in $HepG_2$ cells. (**a**) MTT assay of $HepG_2$ cells after 0–150 μM EGCG treatment (with FBS) for 24, 48, and 72 h. $^*P<0.05$ ($t=2.72$ for 24 h, $t=2.83$ for 48 h) and $^{**}P<0.01$ ($t=5.30$ for 72 h), the treated groups were compared with an untreated control (considered to be 100% viable). The data are presented as mean ± S.D. derived from three independent experiments. (**b**) Western blot assay of intracellular and extracellular AFP. $HepG_2$ cells were treated in the absence or presence of 25 and 50 μM EGCG for 24 h. (**c**) $HepG_2$ cells were incubated with or without 50 μM EGCG for 0–6 h, and intracellular and extracellular protein were subjected for western blotting analysis. (**d**) $HepG_2$ cells were treated with 0, 25, and 50 μM EGCG for 24 h, respectively, and stained with AFP-specific primary antibody and CY3-conjugated secondary antibody. Yellow arrows: aggregated AFP protein (×40)

the influence of EGCG on AFP secretion. At concentrations below the 50 μM threshold, EGCG significantly reduced the extracellular AFP level in a dose-dependent trend after 24 h treatment (Figure 1b). To a less extent, the elevation of intracellular AFP levels in $HepG_2$ cells depended on EGCG dose during incubation (Figure 1b). EGCG-mediated inhibition of AFP secretion was also time-dependent, occurring within 0.5 h, but lasting up to 6–24 h (Figure 1c). Immunocytochemistry analysis revealed that EGCG treatment resulted in cytoplasmic AFP aggregates manifesting as numerous 'puncta' structures in HepG2 cells (Figure 1d). Taken together, these experimental data suggested that EGCG treatment caused cytoplasmic AFP aggregation, and inhibited AFP secretion in $HepG_2$ cells.

EGCG induces mitochondria and cytoskeleton damage. To gain insight into the mechanism of EGCG-mediated inhibition of AFP secretion, we examined mitochondrial membrane potential and cytoskeleton structure by fluorescence-labeling. In normal healthy cells, the JC-1 molecular probe permeated into the mitochondrial matrix to form JC-1 aggregates that produced red fluorescence. When the mitochondrial potential decreased, such as in the case of apoptosis onset, the JC-1 molecular probe could not enter the mitochondria and emitted a green fluorescence instead. In the presence of 25 and 50 μM EGCG, only short (0.5 h) exposure could result in a rapid decrease of red fluorescence, which became further pronounced as incubation time progresses to 2 and 4 h, indicating that EGCG stimulated the quick decrease of mitochondrial potential (Supplementary Figure S2A). In comparison with the untreated control where the actins in the green-labeled cytoskeleton were observably continuous, some cytoskeleton structures appeared cloddy after treatment with 25 and 50 μM EGCG for 4 h, indicating the interruption of normal actin structure and precipitation of dysregulated actin aggregate by EGCG (Supplementary Figure S2B)

EGCG promoted LC3-II production and autophagic AFP degradation. Consistent with a previous report,[21] EGCG elevated LC3-II production in non-transfected $HepG_2$ cells (Figure 2a). Moreover, EGCG induced the formation of LC3-containing cytoplasmic vesicles in GFP-LC3-transfected $HepG_2$ cells (autophagosomes, Figure 2c, yellow arrow). Similarly, monodansylcadaverine (MDC) nonspecific stain had also shown the autophagic vacuoles (Figure 2b, yellow arrow). Thus, EGCG could increase LC3-II production and stimulate autophagy. To further test the possibility of autophagic degradation gradually eliminating the AFP aggregates, we determined the colocalization of AFP aggregates in autophagosomes. As we predicted, many cytoplasmic AFP 'puncta' appeared colocalizing with LC3-containing cytoplasmic vesicles after 24 h treatment with 25 μM EGCG (Figure 2c). Furthermore, the blockage of autophagy with 3-methyladenine (3-MA), a specific inhibitor of autophagy-regulating molecule, could further promote the accumulation of cytoplasmic AFP, simultaneously reducing LC3-I and LC3-II levels (Figure 2d). These results collectively suggest that EGCG-mediated AFP aggregation may facilitate autophagic degradation in HepG2 cells.

Spontaneous dimerization of LC3-I in pure water impedes formation of LC3-II complex. The effect of EGCG on the dimerization of LC3-I proteins and its potential influence on the formation of LC3-II complex were furtherly explored with all-atom molecular dynamic (MD) simulations. In control simulations, the two individual LC3-I proteins (independent of the initial orientation, Figures 3a and b) aggregated to a stable and morphologically similar dimer in all trajectories (Figure 4, left column). Time-based evolution of the distance between the center of mass (COM) of two proteins reveals the quick nature of the dimerization process (Supplementary Figure S3). The dimerization patterns for all control simulations are very similar, that is, the N-β_2 and N-α_2 regions in the N-terminal region of a LC3-I protein bind to the C-β_1 region in the C-terminal region of another LC3-I protein (Figure 4 and Supplementary Figure S4). The formed dimers in pure water were structurally closed, with at least one Gly-120 site on the interface of two LC3-I proteins completely harbored and inaccessible for DSPE. Numerous studies have fully addressed the role of Gly-120 in the formation of LC3-II complex,[22–24] with the conjugation of Gly-120 site of LC3-I protein to DSPE through an amide bond being the most important step.[22] Therefore, in pure water, dimerization of LC3-I proteins is unfavorable for the formation of LC3-II complex.

EGCG promoted LC3-II production by inhibiting dimerization of LC3-I. After adding EGCG, the dimerization of LC3-I undergoes a noticeable delay or somewhat inhibition. For example, in some EGCG+ simulations, the two dimers remaining separated from each other till the end of the simulations (run2 in EGCG-i and EGCG-ii system, the middle picture in right column of Figure 4 and Supplementary Figure S3, respectively). The much larger averaged COM distance between two monomers in EGCG-ii systems ($\sim 3.57 \pm 0.49$ nm) in comparison with control systems ($\sim 2.96 \pm 0.50$ nm) also demonstrated the inhibition of LC3-I protein dimerization (Supplementary Figure S3). In run1 of the EGCG-i system (the purple curve in Supplementary Figure S3), the COM distance between two monomers largely fluctuates until $t > 70$ ns, when the two monomers begin to approach each other. In run2 (the green curve in Supplementary Figure S3, EGCG-i system), the two monomers did not even show any dimerizing tendency. Taken together, the dimerization of LC3-I was significantly inhibited. Consequently, the Gly-120 site in the C-terminal region of LC3-I protein is freely open to DSPE (the right column of Figure 4 and Supplementary Figure S4), which in turn can promote the formation of the LC3-II complex and result in the degradation of AFP aggregates by autophagy.

The underlying molecular mechanisms for EGCG inhibited dimerization of LC3-I. Furthermore, to gain a deeper insight into molecular mechanisms of EGCG-stimulated autophagosome formation, namely, the interaction between EGCG with LC3-I protein, the residual contact probability between two LC3-I monomers were analyzed. The formation of many stable salt-bridges between two proteins, particularly Glu-117 with Lys-48, Lys-50, Lys-65 or Arg-69, Arg-70, mainly triggered LC3-I dimerization (Figure 5a). Figure 5b shows a typical LC3-I protein dimer stabilized by a salt-bridge

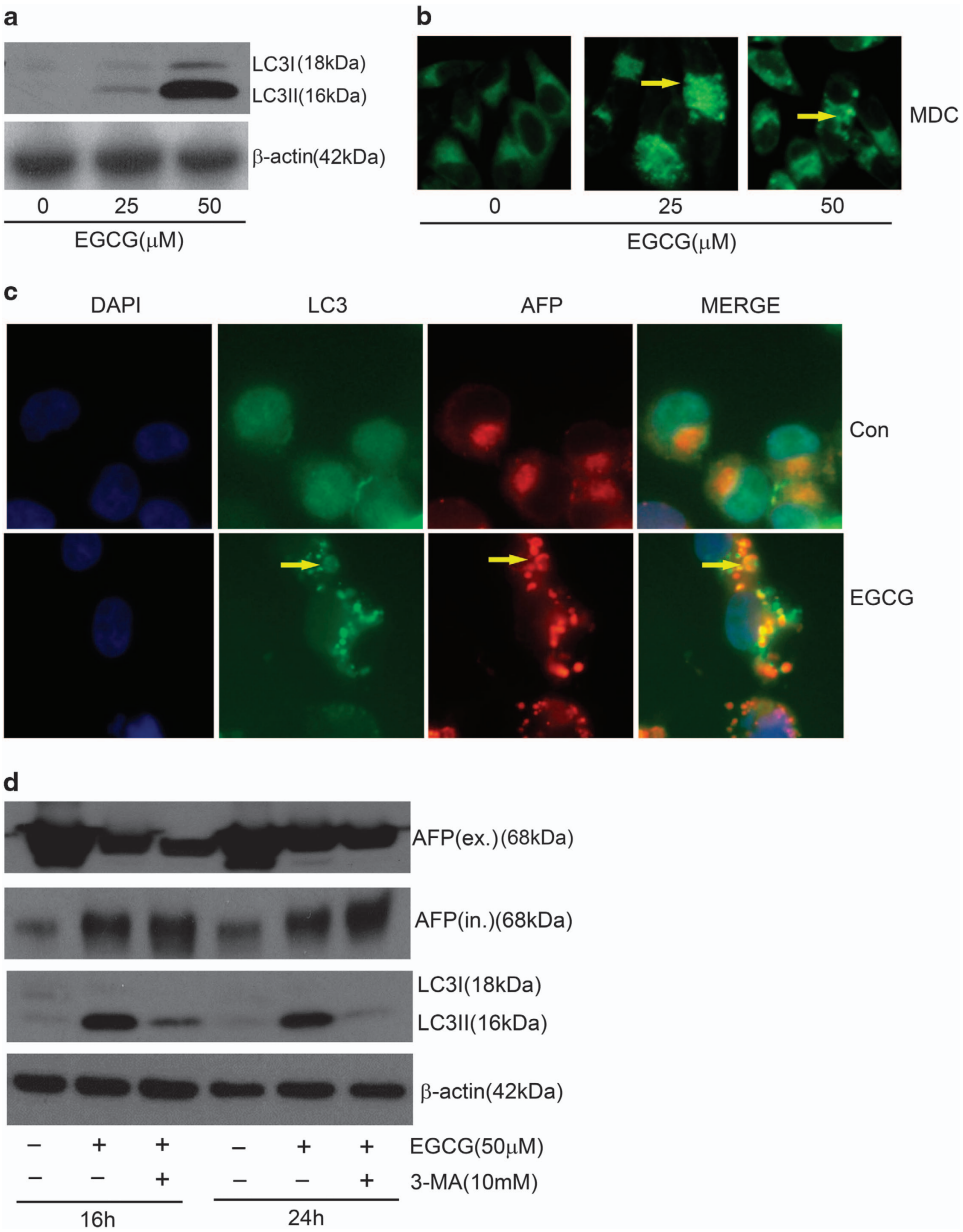

Figure 2 EGCG induced intracellular AFP degradation through autophagy in $HepG_2$ cells. (**a**) $HepG_2$ cells were stimulated with 25 and 50 μM EGCG for 24 h. The 18-kDa cytosolic LC3-I and 16-kDa lipidated autophagosome-bound LC3-II was analyzed by the western blot method. (**b**) $HepG_2$ cells were stimulated with 25 and 50 μM EGCG for 24 h, and then stained with acidotropic MDC dye to visualize autophagosomes (yellow arrow: autophagosomes) (×40). (**c**) GFP-transfected $HepG_2$ cells were stimulated with 50 μM EGCG for 24 h. Cytoplasmic aggregated AFP were partly colocalized with LC3-containing vesicles (as shown by yellow arrows) (×60). (**d**) EGCG enhanced intracellular AFP level in the presence of 3-MA. $HepG_2$ cells were stimulated with 50 μM EGCG for 16 and 24 h, and 10 mM 3-MA was added at 4 h before EGCG treatment. Western blot analysis was conducted to determine extracellular, intracellular LC3, and AFP level with reference to β-actin

between Glu-117 and Arg-69, which directly induces the complete harboring of the Gly-120 site on the interface of two LC3-I proteins, thus preventing access of DSPE, and hindering the formation of LC3-II complex. Upon addition of EGCG, the residual contact probability map between two proteins further illustrates the suppression of salt-bridge formation during protein dimerization (Figure 5a), particularly on the residues around Glu-117 (Figures 5c and d). Thus, the Gly-120 site in the C-terminal region of LC3-I protein is released to DSPE. The capability of EGCG inhibiting LC3-I dimerization mainly arises from the high binding affinity of the former with the charged and polar residues of the latter through electrostatic attractions and hydrogen bonding, respectively (Figures 5e–g). The coating of EGCGs (especially the charged sites) acts as a shield against long-range electrostatic interactions between two proteins and inhibits the dimerization of proteins.

Discussion

Accumulating scientific reports have extensively studied EGCG, the most active and abundant component of green

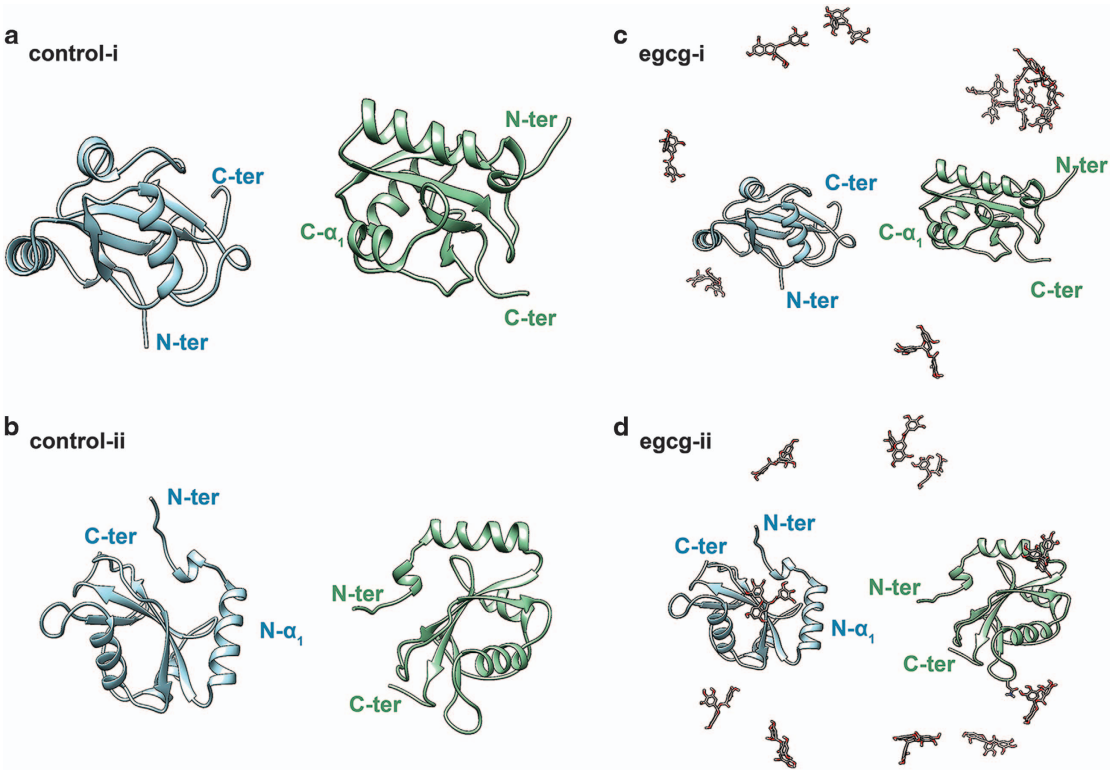

Figure 3 The initial configurations for molecular dynamic simulations consisting of LC3-I protein and EGCG molecular in the water solvated system. LC3-I protein inserted in pure water marked as the control system: (**a**) control-i, in the C-terminal region of two LC3-I proteins faced each other; (**b**) control-ii system, in the N-terminal region of two LC3-I proteins faced each other. Ten EGCG molecules were randomly placed into (**a**) and (**b**) systems, yielding two corresponding EGCG+ system: (**c**) EGCG-i and (**d**) EGCG-ii, respectively. For clarity, water molecules and ions are not shown. Two LC3-I protein are shown as light green and light blue NewCartoon representation. EGCG molecules colored by element, carbon atoms are gray, oxygen atoms are red, and hydrogen atoms are white

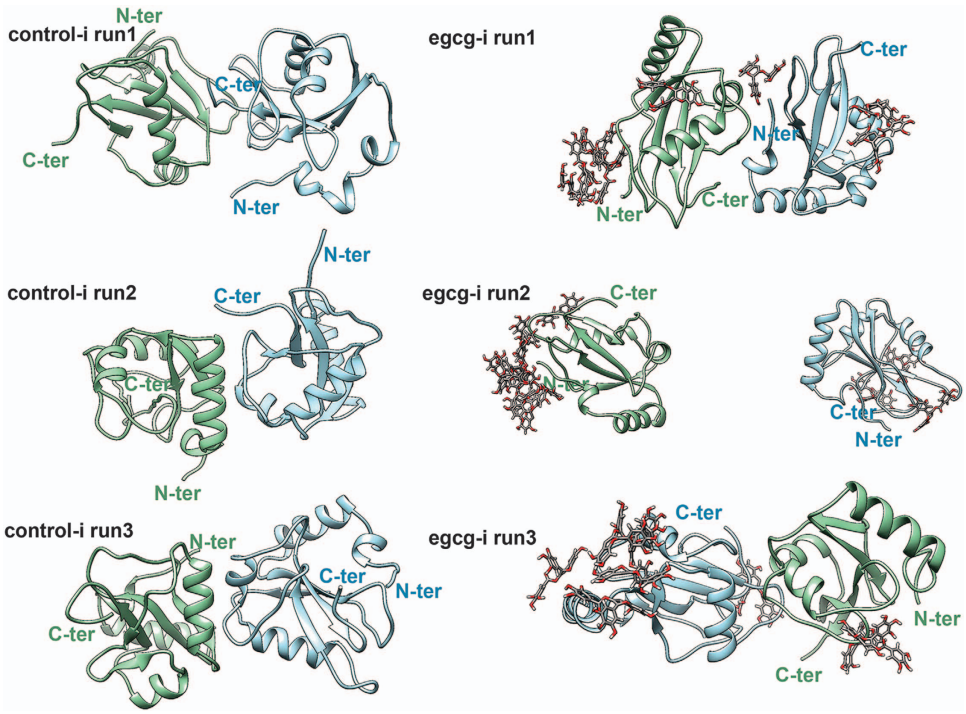

Figure 4 The three final snapshots (at $t = 100$ ns) of control-i (left column) and EGCG-i system (right column, system depicted in Figure 3) from different initial phase space. LC3-I proteins are displayed with different color to distinguish them, and the terminal of proteins were labeled as N-ter and C-ter for the same purpose

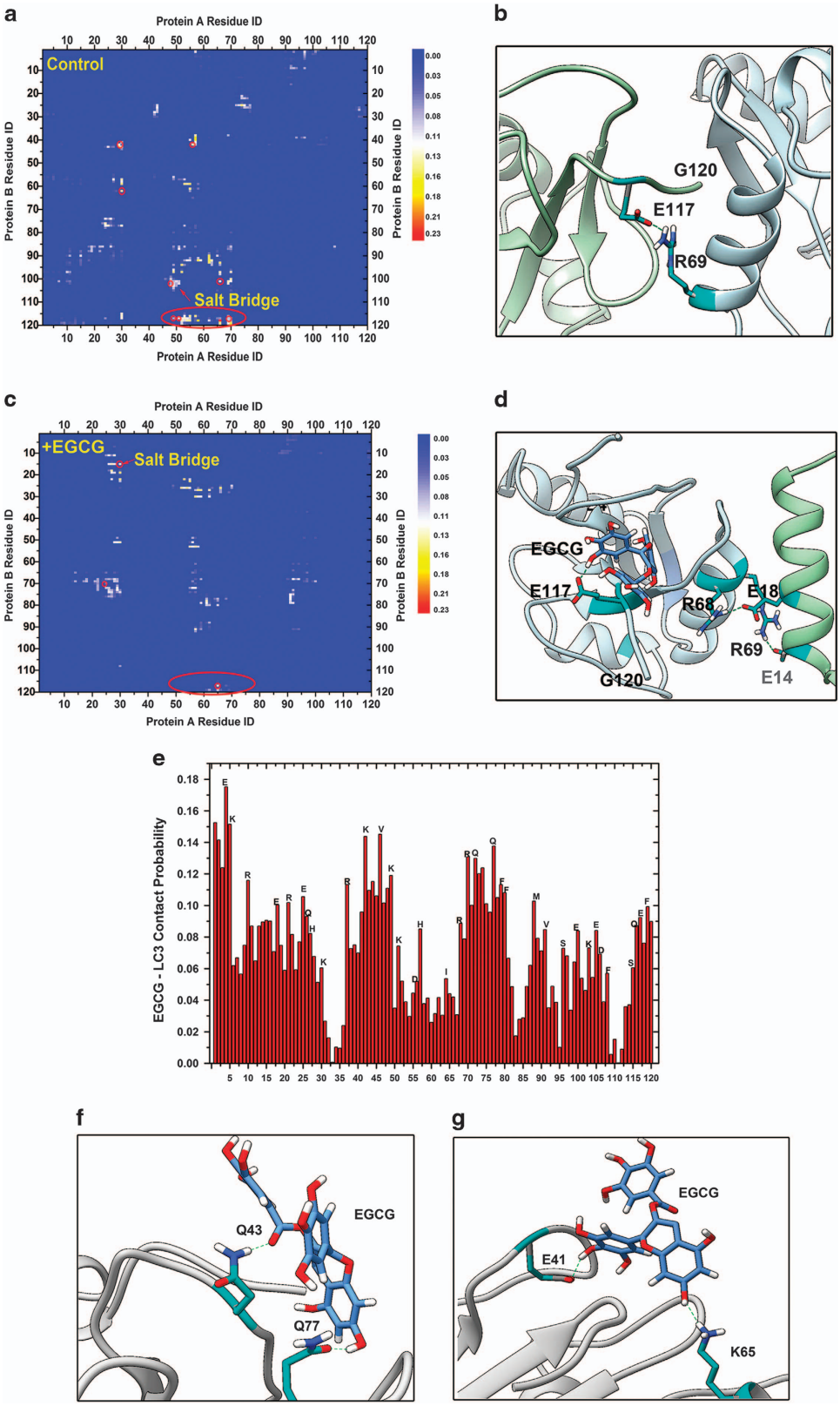

Figure 5 The underlying molecular mechanisms for EGCG to inhibit the dimerization of LC3-I protein. The residual contact probability map of two LC3-I protein (**a**) is counted over all control systems, and (**c**) is counted over all the EGCG+ systems. The contact cutoff is defined as 0.5 nm. (**b** and **d**) The corresponding typical configurations highlighted by the red circle in (**a**) and (**b**), respectively. (**e**) The contact probability of EGCG with LC3-I protein (cutoff is 0.5 nm). The typical configurations for EGCG interacting with the polar residues (**f**), and the charged residues (**g**) through hydrogen bonds

tea, for its anticancer effect. Previously, the effect of the apoptotic mechanism stimulated by lower mitochondrial membrane potential and the G0/G1 phase cell cycle arrest was previously demonstrated in HCC.[25] In addition, other reports have indicated that targeting the EP(1) receptor[26] and copper accumulation[27] can mediate anti-HCC activities. In our study, EGCG at concentrations below 50 μM could inhibit $HepG_2$ cell growth slightly better than higher EGCG concentrations of 50–100 μM under the same conditions (Figure 1a). Thus, we proposed that EGCG concentrations below 50 μM should be capable of evoking protective mechanisms that battle against its damaging effect.

In the present study, EGCG diminished the secretion of AFP (Figures 1b and c). AFP seemed trapped in the cytoplasm of $HepG_2$ cells after EGCG treatment (Figure 1d). As a universal biomarker of HCC, AFP is generally detectable in patients with hepatological diseases. We hypothesized that EGCG possibly inhibited AFP secretion by causing an energy shortage in the mitochondria and a deficiency of motion-dependent matrix in the cytoskeleton (Supplementary Figure S2 and Figure 6). Intriguingly, EGCG lowered the level of secreted osteopontin, a protein similar to AFP, which also mediated HCC metastasis and invasion.[28] Because a previous report demonstrated that secreted AFP could enhance tumor cell proliferation by binding to AFP receptors localized in HCC cell membranes,[29] we considered that the diminished AFP secretion by EGCG should be one of the reasons behind the inhibition of $HepG_2$ growth.

As salvation of dying cells, autophagy participates in numerous cellular events. According to previous studies, the possibility of EGCG promoting or attenuating autophagy remains elusive. Recent studies had indicated that EGCG exhibited an antiautophagic effect through the IL-6/JAKs/STAT3 pathway,[12] or protection of mitochondrial function,[30] benefitting the organism. Paradoxically, EGCG could potentially activate autophagy in certain cases to protect normal cells[31] or sensitize the cancer cells to chemotherapy drugs.[32] EGCG could notably increase autophagosome synthesis instead of inhibiting LC3-II degradation upon adding a proton pump inhibitor, such as bafilomycin A1, at saturating concentrations in raw cells.[21] Our results supported this opinion, and we proposed that autophagy should be one way of degrading intracellular AFP (Figure 6). Several previous studies concluded that cytoplasmic AFP could activate the (PI3K)/AKT pathway,[33] prevent RAR from nuclear translocation, and inhibit the expression of *Fn14* gene,[34] which participates in the regulation of HCC growth. Thus, autophagy is important in complementing the protective effect of EGCG and in fighting against damage.

Our MD simulation further explored the underlying mechanism of EGCG-promoted LC3-II production. It was suggested that EGCG binding to the charged residues or other polar

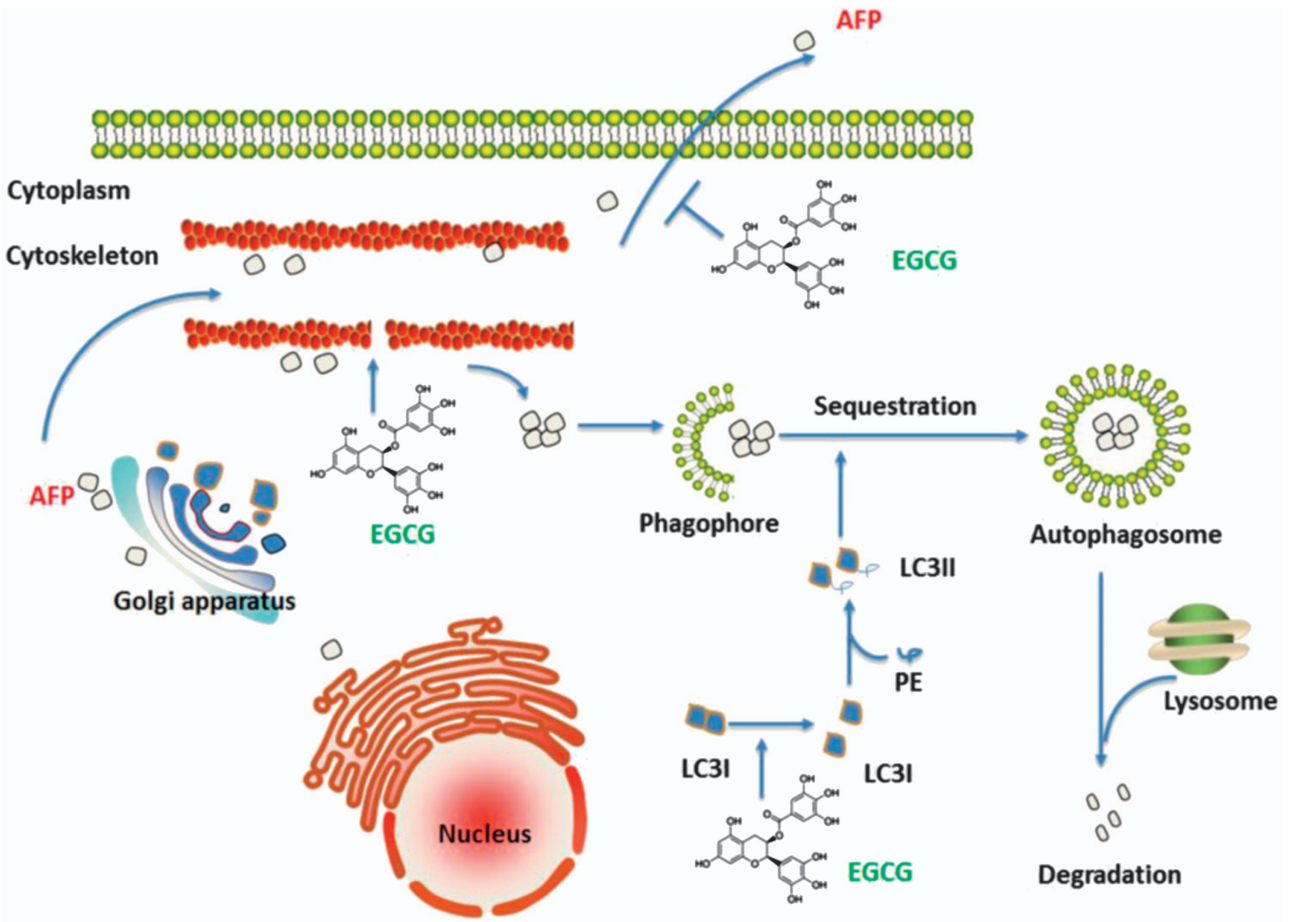

Figure 6 The mechanism of EGCG inhibits AFP secretion and promotes its degradation by autophagy

residues of LC3-I protein can effectively hinder the long-range electrostatic interactions between two monomer proteins, and thereby inhibit the dimerization of LC3-I. Inhibition of the dimerization of proteins leads the pivotal Gly-120 site in the C-terminal region of LC3-I more exposed to the other molecules such as DSPE, which in turn can evaluate the production of LC3-II complex (Figure 6). Historically, there are numerous studies discussing about the interaction of EGCG with proteins. It was illustrated that EGCG possessed the therapeutic potential against Alzheimer's disease, and had been recognized as an antiamyloid agent.[35,36] In addition, EGCG inhibited the aggregation of tau into toxic oligomers, and protected the neuronal model cells.[37] Furthermore, we also found that EGCG could firmly bind to HMGB1 near Cys-106, and subsequently stimulated large HMGB1 conformational change.[38] All these indicted that EGCG possessed unique functions, which determined its diverse applications in biomedical field.

In conclusion, we deduced the complex biochemistry and physical reactions in human HCC $HepG_2$ cells treated with EGCG at concentrations below 50 μM. On the one hand, EGCG displayed its cytotoxic effects by inhibiting AFP secretion and promoting intracellular aggregation. On the other hand, EGCG also evoked autophagy to degrade the AFP aggregate and to protect cells from damage. Furthermore, our findings provide a novel mechanism on the autophagic function of EGCG towards AFP and the unique advantages of autophagy in the prevention and treatment of liver cancer, supporting the health benefits of green tea.

Materials and Methods

Reagents. EGCG (≥98% purity), 3-MA and 4′,6-diamidino-2-phenylindole (DAPI), MDC, and MTT were provided by Sigma (St. Louis, MO, USA). EGCG was dissolved in deionized water to prepare 10 mM stock solutions at − 20 °C. Dulbecco's modified Eagle's medium (DMEM), OPTI-MEM I medium and fetal bovine serum (FBS) were purchased from Gibco (Grand Island, NY, USA). AFP and LC3 mouse monoclonal antibody were purchased from Santa Cruz Biotechnology (Santa Cruz, CA, USA). Anti-β-actin was obtained from Sigma-Aldrich (St. Louis, MO, USA). Horseradish peroxidase-conjugated anti-rabbit or anti-mouse secondary antibodies were purchased from Wuhan Boster Biological Engineering Co. (Wuhan, China). Cy3-labeled anti-mouse antibody, Actin-Tracker Green, Mitochondrial Membrane Potential Assay Kit with JC-1 and the BCA Protein Assay Kit were purchased from Beyotime Institute of Biotechnology (Beijing, China).

Cell culture. $HepG_2$ cells were obtained from the American Type Culture Collection (Rockville, MD, USA). Cells were maintained in DMEM (Gibco, Shanghai, China), supplemented with 10% fetal bovine serum (FBS), L-glutamine (5 mmol/l), penicillin (100 U/ml), and streptomycin (100 U/ml) (Invitrogen, Carlsbad, CA, USA), at 37 °C in a humidified 5% CO_2 atmosphere.

Transfection and establishment of stable cell lines. $HepG_2$ cells were transfected with GFP-LC3 plasmid (obtained from Dr. N Tony Eissa, Department of Medicine, Baylor College of Medicine, Houston, TX, USA) by Lipofectamine 2000 (Life Technologies Inc., Carlsbad, CA, USA), with an aim to detect specific autophagosome by using LC3-transfected $HepG_2$ cells, which could help reflect the level of autophagy. Briefly, the Lipofectamine reagent (1 : 25, v/v) and the GFP-LC3 plasmid (1.0 μg/1000 μl) were diluted by the serum-reduced OPTI-MEM I medium in separate Eppendorf tube. Then, they were mixed at a 1 : 1 ratio (v/v), and then incubated at room temperature for 10 min. $HepG_2$ cells ($1–2\times10^6$ cells) were seeded onto 100-mm tissue culture Petri dish (10 ml) and cultured in the DMEM/10% FBS/2 mM glutamine until reaching 70–80% confluency, and replaced with fresh OPTI-MEM I medium (10 ml) after two washes with prewarmed OPTI-MEM I medium. The GFP-LC3 plasmid/Lipofectamine mixture (5.0 ml, containing 2.5 μg plasmid DNA) was added to the $HepG_2$ cell culture, and incubated for 12–16 h. Afterwards, $HepG_2$ cells stably expressing GFP-LC3 were selected and maintained in DMEM/10%FBS/2 mM glutamine supplemented with geneticin (600 μg/ml; Gibco, China).

Cell viability assay. MTT assay was performed to measure cell viability. Generally, $HepG_2$ cells were seeded into 96-well cell culture plates at the density of 6000 cells/well. EGCG at different concentrations (0–150 μM) were added to cells for 24, 48, and 72 h incubation. Then, the treated cells were incubated with 20 μl MTT (5 mg/ml) in each well for another 4 h. The supernatant was removed and 150 μl DMSO was added into each well, and after oscillating for a 10 min duration, the absorbance (OD value) was determined by a Micro Plate Reader (Bio-Tek Instruments Inc., Winooski, VT, USA) at 570 nm, with the absorbance at 630 nm as the background correction. The effect on cell proliferation was expressed as the percent cell viability. Untreated cells were taken as 100% viable.

Mitochondrial membrane potential assay. JC-1 fluorescence probe was used to test the mitochondrial membrane potential. $HepG_2$ cells were seeded into 6-well cell culture plates and incubated with 0, 25, and 50 μM EGCG for 0.5, 2, and 4 h, respectively, when cells were attached onto the bottom of the plates. Then, after extensively washing with sterile PBS, the prepared 1 ml JC-1 working buffer mixed with 1 ml cell culture medium (containing FBS) were added into each well at 37 °C for 20 min. JC-1 dyeing buffer was discarded and the cells were washed with ice-cold PBS for two times to avoid the cytotoxic effect of JC-1. Later, the fresh medium was readded and images were captured using a fluorescence microscope (Carl Zeiss Microimaging Inc., Göttingen, Germany).

Visualization of cytoskeleton. $HepG_2$ cells were plated onto circular glass coverslips and incubated with different concentrations of EGCG (0, 25, and 50 μM) for 6 h. Afterwards, cells were washed with PBS and fixed with freshly prepared 3.7% methanal for 10 min at room temperature, and permeabilized with 0.1% Triton X-100 in PBS three times for the next 5 min. Diluted Actin-Tracker Green (1 : 100) was added and incubated for 30 min at 37 °C. Then, the green actin cells inside was captured by a fluorescence microscope (Carl Zeiss Microimaging).

Visualization of autophagosomes. $HepG_2$ cells stably transfected with GFP-LC3 were treated in the absence or presence of EGCG for 24 h. And, the presence of GFP-LC3 punctate structures in cells was examined under a fluorescence microscope. In addition, MDC dyeing method was also used to detect unspecific autophagosomes. First, MDC was dissolved in DMSO to prepare 50 mM stock solution and diluted at 1:1000 for working solution. $HepG_2$ cells were treated with 0, 25, and 50 μM EGCG for 24 h, respectively. Then, cells were washed with PBS and dyed with MDC working solution for 30 min at room temperature. The images were captured by a fluorescence microscope (Carl Zeiss Microimaging).

Immunofluorescence analysis. To visualize AFP localization, $HepG_2$ cells were plated onto circular glass coverslips and incubated in the presence or absence of EGCG (25 and 50 μM) for 24 h. To detect the colocalization of AFP and autophagosome, GFP-LC3-labeled $HepG_2$ cells was treated with 50 μM EGCG for 24 h. The immunofluorescence analysis was conducted as described previously.[39] Briefly, cells were fixed with freshly prepared 2% formalin for 20 min at room temperature, and were permeabilized with 0.1% Triton X-100 in PBS for next 10 min. AFP antibody was added at 1 : 1000 and incubated overnight at 4 °C, followed by a mouse IgG-CY3 secondary antibody (Beyotime, Jiangsu, China) at 1 : 1000 for 1 h. The nucleus was stained with 5 μg/ml DAPI at room temperature for 30 min. Images were captured using a fluorescence microscope (Carl Zeiss Microimaging).

Western blotting analysis. $HepG_2$ cells were incubated with or without 25 and 50 μM EGCG for 24 h. To test the secreted AFP content in the medium, the culture supernatant was concentrated by an ultrafiltration device (Amicin Ultra-4 Centrifugal Filter Units; Millipore Co., Billerica, MA, USA), and then collected to conduct western blot analysis. Cellular total protein was extracted from cells using an IP lysing buffer (Beyotime, Jiangsu, China) containing (25 mg/ml) protease inhibitor (complete ULTRA Tablets; Roche, Mannheim, Germany). Protein concentration was determined by the BCA Protein Assay Kit (Beyotime, Jiangsu, China). The antibodies of AFP and LC3 were diluted at concentration 1 : 1000, and the western blot analysis was conducted as described previously.[39] In addition, for testing the autophagic flux, we evaluated the LC3-II turnover after the treatment of EGCG in the absence or presence of an autophagy inhibitor, 3-MA. 10 mM 3-MA

was added at 4 h before $HepG_2$ cells were stimulated with 50 μM EGCG for 16, 24 h, respectively. Cells were harvested and assayed for the ratio between the 18-kDa cytosolic LC3-I and 16-kDa lipidated autophagosme-bound LC3-II.

Molecular dynamics simulations. The crystal structure of LC3-I protein was obtained from the Protein Data Bank (PDB code: 1V49[40]). Analyses of electrostatic surface potential (ESP) demonstrate that the LC3-I protein has large molecular polarity and distinctive electrostatic potential surface, with the positive charged region contributed by the N-terminal region, and the negative charged region contributed by the C-terminal region (see Supplementary Figure S1) (see below). Therefore, to avoid the quick approaching of two LC3-I proteins induced by the polarity of protein, and enrich sampling, the initial configurations of control systems were set to the C-terminal region (control-i system) or the N-terminal region (control-ii system) of two LC3-I proteins facing each other (see below). Initially, for both systems, the closest distances between any heavy atoms of two proteins were settled larger than 1.0 nm. Then, both protein dimers were solvated into a rectangular water box with a size of (13.64 nm × 10.51 nm × 13.32nm) and (13.13 nm × 11.39 nm × 9.56 nm) for control-i and control-ii systems (see below), respectively. Two Cl^- ions were added to neutralize both systems. After an equilibrium procedure (more below), 10 EGCG molecules were randomly introduced into the simulation boxes of control-i and control-ii systems, yielding two new EGCG+ systems (denoted by EGCG-i and EGCG-ii systems (see below)). These two EGCG+ systems were used to study the effect of EGCG on the dimerization of the LC3-I protein.

The molecular dynamic (MD) simulations were conducted with the software package GROMACS version 4.6.7.[41] The protein ESP was depicted with APBS server.[42] Chimera program[43] was used for trajectory visualization and analysis. The GROMOS96 53a6 force field[44] was used for proteins. The force field parameters for EGCG were adopted from a previous literature.[45] The simple point charge model was used for water.[46] The two control systems were subjected to a 20 000 steps energy minimization, followed by a further 2 ns NVT relaxation, with the temperature maintained at 300 K using *v*-rescale thermostat.[47] The resulting two EGCG+ systems were re-equilibrated with the similar equilibration protocol as the two control systems. Then, for each system, 3 × 100 ns independent production runs were performed. The total aggregated simulation time was larger than 1.2 μs. During the production runs, an NPT ensemble was used, with the temperature maintained at 300 K using v-rescale thermostat, and the pressure at 1 bar via Parrinello–Rahman coupling scheme.[48] A time step of 2.0 fs was used, and data were collected every 5 ps. For all of our simulations, periodic boundary conditions were applied in all directions. The long-range electrostatic interactions were treated with the PME method,[49] and the van der Waals interactions were calculated with a cutoff distance of 1.0 nm. All solute bond lengths were maintained constant at their equilibrium values with the LINCS algorithm,[50] and water geometry was also constrained using the SETTLE algorithm.[51]

Statistical analysis. Data are expressed as mean ± S.D. of at least three independent experiments ($n = 3+$). Statistical comparisons of the experimental results between the treated group and the control group were made using the two-tailed Student's *t*-test. All statistical tests were performed using SPSS version 17.0 (IBM, Chicago, IL,USA). *P*-value ≤ 0.05 between groups was considered significant.

Conflict of Interest

The authors declare no conflict of interest.

Acknowledgements. We thank Bruce Berne, Hongsuk Kang, Xuanyu Meng, and Tanya Singh for helpful discussions. This work was supported by the National Natural Science Foundation of China (Grants Nos. 11404233, 81703159, 11374221, and 21320102003) and the Natural Science Foundation of Jiangsu Province (Grants Nos. 14KJB310018 and BK20161213), Postdoctoral research funding plan in Jiangsu province (1601121C), the Priority Academic Program Development of Jiangsu Higher Education Institutions (PAPD), Jiangsu Provincial Key Laboratory of Radiation Medicine and Protection, and the Program of Suzhou Scientific and Technology (SYS201511). This work was also supported, in part, by the US National Institute of General Medical Sciences (NIGMS, R01GM063075) and the National Center of Complementary and Alternative Medicine (NCCAM, R01AT05076).

Author contributions

LZ, ZY, and RZ conceived and designed the research. LZ performed the experiments. SL and ZY carried out the molecular dynamics simulations. LZ, SL, ZY, and RZ analyzed the data. LZ, SL, ZY, and RZ cowrote the manuscript. All authors discussed the results and commented on the manuscript.

Publisher's Note

1. Zhang XL, Cheng XP, Yu L, Yang JS, Calvo R, Patnaik S *et al.* MCOLN1 is a ROS sensor in lysosomes that regulates autophagy. *Nat Commun* 2016; **7**: 12109.
2. Cinque L, Forrester A, Bartolomeo R, Svelto M, Venditti R, Montefusco S *et al.* FGF signalling regulates bone growth through autophagy. *Nature* 2015; **528**: 272–275.
3. Koren I, Kimchi A. Promoting tumorigenesis by suppressing autophagy. *Science* 2012; **338**: 889–890.
4. Huang YC, Li YM, Chen Y, Pan M, Li YT, Yu L *et al.* Synthesis of autophagosomal marker protein LC3-II under detergent-free conditions . *Angew Chem Int Edit* 2013; **52**: 4858–4862.
5. Ju J, Hong J, Zhou JN, Pan Z, Bose M, Liao J *et al.* Inhibition of intestinal tumorigenesis in Apcmin/+ mice by (−)-epigallocatechin-3-gallate, the major catechin in green tea. *Cancer Res* 2005; **65**: 10623–10631.
6. Bettuzzi S, Brausi M, Rizzi F, Castagnetti G, Peracchia G, Corti A. Chemoprevention of human prostate cancer by oral administration of green tea catechins in volunteers with high-grade prostate intraepithelial neoplasia: a preliminary report from a one-year proof-of-principle study. *Cancer Res* 2006; **66**: 1234–1240.
7. Lu YP, Lou YR, Xie JG, Peng QY, Liao J, Yang CS *et al.* Topical applications of caffeine or (−)-epigallocatechin gallate (EGCG) inhibit carcinogenesis and selectively increase apoptosis in UVB-induced skin tumors in mice. *Proc Natl Acad Sci USA* 2002; **99**: 12455–12460.
8. Granja A, Pinheiro M, Reis S. Epigallocatechin gallate nanodelivery systems for cancer therapy. *Nutrients* 2016; **8**: 307.
9. Chung JE, Tan S, Gao SJ, Yongvongsoontorn N, Kim SH, Lee JH *et al.* Self-assembled micellar nanocomplexes comprising green tea catechin derivatives and protein drugs for cancer therapy. *Nat Nanotechnol* 2014; **9**: 907–912.
10. Irimie AI, Braicu C, Zanoaga O, Pileczki V, Gherman C, Berindan-Neagoe I *et al.* Epigallocatechin-3-gallate suppresses cell proliferation and promotes apoptosis and autophagy in oral cancer SSC-4 cells. *OncoTargets Ther* 2015; **8**: 461–470.
11. Chen L, Ye HL, Zhang G, Yao WM, Chen XZ, Zhang FC *et al.* Autophagy inhibition contributes to the synergistic interaction between EGCG and doxorubicin to kill the hepatoma Hep3B cells. *PLoS ONE* 2014; **9**: e85771.
12. Li S, Xia Y, Chen K, Li J, Liu T, Wang F *et al.* Epigallocatechin-3-gallate attenuates apoptosis and autophagy in concanavalin A-induced hepatitis by inhibiting BNIP3. *Drug Des Devel Ther* 2016; **10**: 631–647.
13. Hung CH, Hu TH, Lu SN, Kuo FY, Chen CH, Wang JH *et al.* Circulating microRNAs as biomarkers for diagnosis of early hepatocellular carcinoma associated with hepatitis B virus. *Int J Cancer* 2016; **138**: 714–720.
14. Lu Y, Zhu MY, Li W, Lin B, Dong X, Chen Y *et al.* Alpha fetoprotein plays a critical role in promoting metastasis of hepatocellular carcinoma cells. *J Cell Mol Med* 2016; **20**: 549–558.
15. Ryerson AB, Eheman CR, Altekruse SF, Ward JW, Jemal A, Sherman RL *et al.* Annual Report to the Nation on the Status of Cancer, 1975–2012, featuring the increasing incidence of liver cancer. *Cancer* 2016; **122**: 1312–1337.
16. Fang ZL, Fang N, Han XN, Huang G, Fu XJ, Xie GS *et al.* Effects of AFP gene silencing on Survivin mRNA expression inhibition in HepG2 cells. *Genet Mol Res* 2015; **14**: 3184–3190.
17. Houessinon A, Gicquel A, Bochereau F, Louandre C, Nyga R, Godin C *et al.* Alpha-fetoprotein is a biomarker of unfolded protein response and altered proteostasis in hepatocellular carcinoma cells exposed to sorafenib. *Cancer Lett* 2016; **370**: 242–249.
18. Ju HX, Cui YB, Chen ZQ, Fu QP, Sun MZ, Zhou Y. Effects of combined delivery of extremely low frequency electromagnetic field and magnetic Fe_3O_4 nanoparticles on hepatic cell lines. *Am J Transl Res* 2016; **8**: 1838–1847.
19. Nishida H, Omori M, Fukutomi Y, Ninomiya M, Nishiwaki S, Suganuma M *et al.* Inhibitory effects of (−)-epigallocatechin gallate on spontaneous hepatoma in C3H/HeNCrj mice and human hepatoma-derived PLC/PRF/5 cells. *Jpn J Cancer Res* 1994; **85**: 221–225.
20. Darweish MM, Abbas A, Ebrahim MA, Al-Gayyar MM. Chemopreventive and hepatoprotective effects of Epigallocatechin-gallate against hepatocellular carcinoma: role of heparan sulfate proteoglycans pathway. *J Pharm Pharmacol* 2014; **66**: 1032–1045.
21. Li W, Zhu S, Li J, Assa A, Jundoria A, Xu J *et al.* EGCG stimulates autophagy and reduces cytoplasmic HMGB1 levels in endotoxin-stimulated macrophages. *Biochem Pharmacol* 2011; **81**: 1152–1163.
22. Kabeya Y, Mizushima N, Ueno T, Yamamoto A, Kirisako T, Noda T *et al.* LC3, a mammalian homologue of yeast Apg8p, is localized in autophagosome membranes after processing. *EMBO J* 2000; **19**: 5720–5728.
23. Otomo C, Metlagel Z, Takaesu G, Otomo T. Structure of the human ATG12 similar to ATG5 conjugate required for LC3 lipidation in autophagy. *Nat Struct Mol Biol* 2013; **20**: 59–U79.
24. Huang YC, Li YM, Chen Y, Pan M, Li YT, Yu L *et al.* Synthesis of autophagosomal marker protein LC3-II under detergent-free conditions. *Angew Chem Int Edit* 2013; **52**: 4858–4862.
25. Zhang Y, Duan W, Owusu L, Wu D, Xin Y. Epigallocatechin-3-gallate induces the apoptosis of hepatocellular carcinoma LM6 cells but not non-cancerous liver cells. *Int J Mol Med* 2015; **35**: 117–124.

26. Jin J, Chang Y, Wei W, He YF, Hu SS, Wang D *et al.* Prostanoid EP1 receptor as the target of (−)-epigallocatechin-3-gallate in suppressing hepatocellular carcinoma cells *in vitro*. *Acta Pharmacol Sin* 2012; **33**: 701–709.
27. Farhan M, Rizvi A, Naseem I, Hadi SM, Ahmad A. Targeting increased copper levels in diethylnitrosamine induced hepatocellular carcinoma cells in rats by epigallocatechin-3-gallate. *Tumour Biol* 2015; **36**: 8861–8867.
28. Zapf MA, Kothari AN, Weber CE, Arffa ML, Wai PY, Driver J *et al.* Green tea component epigallocatechin-3-gallate decreases expression of osteopontin via a decrease in mRNA half-life in cell lines of metastatic hepatocellular carcinoma. *Surgery* 2015; **158**: 1039–1047.
29. Ji X, Shen Y, Sun H, Gao X. A novel anti-alpha-fetoprotein single-chain variable fragment displays anti-tumor effects in HepG2 cells as a single agent or in combination with paclitaxel. *Tumour Biol* 2016; **37**: 10085–10096.
30. Chen Y, Huang L, Zhang H, Diao X, Zhao S, Zhou W. Reduction in autophagy by (−)-epigallocatechin-3-gallate (EGCG): a potential mechanism of prevention of mitochondrial dysfunction after subarachnoid hemorrhage. *Mol Neurobiol* 2016; **54**: 392–405.
31. Modernelli A, Naponelli V, Giovanna Troglio M, Bonacini M, Ramazzina I, Bettuzzi S *et al.* EGCG antagonizes Bortezomib cytotoxicity in prostate cancer cells by an autophagic mechanism. *Sci Rep* 2015; **5**: 15270.
32. Hu F, Wei F, Wang Y, Wu B, Fang Y, Xiong B. EGCG synergizes the therapeutic effect of cisplatin and oxaliplatin through autophagic pathway in human colorectal cancer cells. *J Pharmacol Sci* 2015; **128**: 27–34.
33. Li M, Li H, Li C, Wang S, Jiang W, Liu Z *et al.* Alpha-fetoprotein: a new member of intracellular signal molecules in regulation of the PI3K/AKT signaling in human hepatoma cell lines. *Int J Cancer* 2011; **128**: 524–532.
34. Wang S, Jiang W, Chen X, Zhang C, Li H, Hou W *et al.* Alpha-fetoprotein acts as a novel signal molecule and mediates transcription of Fn14 in human hepatocellular carcinoma. *J Hepatol* 2012; **57**: 322–329.
35. Palhano FL, Lee J, Grimster NP, Kelly JW. Toward the molecular mechanism(s) by which EGCG treatment remodels mature amyloid fibrils. *J Am Chem Soc* 2013; **135**: 7503–7510.
36. Bieschke J, Russ J, Friedrich RP, Ehrnhoefer DE, Wobst H, Neugebauer K *et al.* EGCG remodels mature alpha-synuclein and amyloid-beta fibrils and reduces cellular toxicity. *Proc Natl Acad Sci USA* 2010; **107**: 7710–7715.
37. Wobst HJ, Sharma A, Diamond MI, Wanker EE, Bieschke J. The green tea polyphenol (−)-epigallocatechin gallate prevents the aggregation of tau protein into toxic oligomers at substoichiometric ratios. *FEBS Lett* 2015; **589**: 77–83.
38. Meng XY, Li B, Liu S, Kang H, Zhao L, Zhou R. EGCG in green tea induces aggregation of HMGB1 protein through large conformational changes with polarized charge redistribution. *Sci Rep* 2016; **6**: 22128.
39. Zhao L, Xu J, Yang Y, Chong Y, Liu C, Jiao Y *et al.* Inhibitory impacts of chemically modified tetracycline-3 and underlying mechanism in human cervical cancer cells. *Anti-cancer Drug* 2013; **24**: 799–809.
40. Kouno T, Mizuguchi M, Tanida I, Ueno T, Kanematsu T, Mori Y *et al.* Solution structure of microtubule-associated protein light chain 3 and identification of its functional subdomains. *J Biol Chem* 2005; **280**: 24610–24617.
41. Hess B, Kutzner C, van der Spoel D, Lindahl E. GROMACS 4: Algorithms for highly efficient, load-balanced, and scalable molecular simulation. *J Chem Theory Comput* 2008; **4**: 435–447.
42. Unni S, Huang Y, Hanson RM, Tobias M, Krishnan S, Li WW *et al.* Web servers and services for electrostatics calculations with APBS and PDB2PQR. *J Comput Chem* 2011; **32**: 1488–1491.
43. Pettersen EF, Goddard TD, Huang CC, Couch GS, Greenblatt DM, Meng EC *et al.* UCSF Chimera—a visualization system for exploratory research and analysis. *J Comput Chem* 2004; **25**: 1605–1612.
44. Oostenbrink C, Villa A, Mark AE, van Gunsteren WF. A biomolecular force field based on the free enthalpy of hydration and solvation: the GROMOS force-field parameter sets 53A5 and 53A6. *J Comput Chem* 2004; **25**: 1656–1676.
45. Liu FF, Dong XY, He LZ, Middelberg APJ, Sun Y. Molecular insight into conformational transition of amyloid beta-peptide 42 inhibited by (−)-epigallocatechin-3-gallate probed by molecular simulations. *J Phys Chem B* 2011; **115**: 11879–11887.
46. Berendsen HJC, Postma JPM, van Gunsteren WF, Hermans J. Interaction models for water in relation to protein hydration. In: Pullman B (ed). *Intermolecular Forces: Proceedings of the Fourteenth Jerusalem Symposium on Quantum Chemistry and Biochemistry*, Jerusalem, Israel, 13–16 April 1981. Springer: Netherlands, Dordrecht, 1981, pp 331–342.
47. Bussi G, Donadio D, Parrinello M. Canonical sampling through velocity rescaling. *J Chem Phys* 2007; **126**: 014101.
48. Parrinello M, Rahman A. Polymorphic transitions in single crystals: a new molecular dynamics method. *J Appl Phys* 1981; **52**: 7182–7190.
49. Darden T, York D, Pedersen L. Particle mesh Ewald: an *N*·log(*N*) method for Ewald sums in large systems. *J Chem Phys* 1993; **98**: 10089–10092.
50. Hess B, Bekker H, Berendsen HJC, Fraaije J. LINCS: a linear constraint solver for molecular simulations. *J Comput Chem* 1997; **18**: 1463–1472.
51. Miyamoto S, Kollman PA. Settle: an analytical version of the SHAKE and RATTLE algorithm for rigid water models. *J Comput Chem* 1992; **13**: 952–962.

Supplementary Information accompanies this paper on Cell Death and Disease website (http://www.nature.com/cddis)